Dimensional measurement sensitivity analysis for a MoSi photomask using DUV reflection scatterfield imaging microscopy

Martin Y. Sohn*[a], Dong Ryoung Lee[a], Bryan M. Barnes[a], Ronald Dixson[a], Richard M. Silver[a], Sang-Soo Choi[b]

[a]Engineering Physics Division, National Institute of Standards and Technology, 100 Bureau Drive, Gaithersburg, MD, USA 20899-8212; [b]PKL-Photronics, 493-3 Sungsung, Cheonan, Choongnam, South Korea 330-300

ABSTRACT

A critical challenge in optical critical dimension metrology, that requires high measurement sensitivity as well as high throughput, is the dimensional measurements of features sized below the optical resolution limit. This paper investigates the relationships among dimensional sensitivity and key illumination beam conditions (e.g., angular illumination, partial coherence) for photomask feature characterization. Scatterfield images at the edge areas of multiple line structures on a Molybdenum Silicide (MoSi) photomask are analyzed to establish sensitivity to dimensional changes. Actinic scatterfield imaging experiments for these features are performed using the NIST 193 nm Scatterfield Microscope, designed to enable engineered illumination beams at the target. Illumination configurations that improve sensitivity are identified from imaging edges of multiple line targets having linewidths and spaces of about 1/3 wavelength.

Keywords: Optical critical dimension metrology, scatterfield imaging microscopy, measurement sensitivity, partial coherence factor, illumination engineering.

1. INTRODUCTION

Achieving higher densities and smaller dimensions in semiconductor manufacturing technology requires continuous advances in measurement technology. Compared to other metrology techniques, optical metrology techniques have been important to the industry because of their nondestructive character, higher speed, and relatively lower cost [1-3]. A key challenge for optical methods is accurate dimensional measurement of ever-decreasing deep subwavelength feature sizes. Characterizing such features requires high measurement sensitivity with low uncertainties as well as high throughput [4].

Optical scatterfield imaging microscopy techniques have enabled the characterization of nanoscale features sized well below the resolution limit with high sensitivity by analyzing far field images formed by light scattered from the features [5-7]. Engineering of the illumination beam is essential for yielding high sensitivity in scatterfield imaging as the characteristics of the scattered light depend not only on the parameters of the features but also strongly on the incident light conditions such as incident angle, angular intensity, polarization and partial coherence.

The National Institute of Standards and Technology (NIST) has developed reflection scatterfield imaging microscopes operating at visible and deep ultra-violet (DUV) wavelengths for the characterization of nanoscale features on both wafers and photomasks. Model-based CD measurements for finite grating structures of sub-20 nm features have been reported using a visible light scatterfield imaging microscope by Fourier domain normalization method for parametric simulations for comparison with experimental results, yielding sub-nanometer uncertainties [8]. The measured intensity profiles showed high ringing effects at the edges of 100-line gratings and interference effects between both edges of 30-line gratings as a small numerical aperture illumination was imposed on the targets. Notable, a low partial coherence factor may have triggered these edge effects and might be related to the sensitivity of the parametric measurements using the scatterfield imaging microscopy technique. From these results, we noticed that both partial coherence, expressed as the illumination numerical aperture (NA) relative to the collection numerical aperture [9], and image quality have been important for high resolution imaging microscopy and for lithography, thus the relationship between the partial coherence and measurement sensitivity for image-based CD metrology warranted further investigation.

* martin.sohn@nist.gov

In this paper, we present a dimensional measurement sensitivity analysis with respect to various illumination conditions as a function of the partial coherence factor using the NIST 193 nm scatterfield imaging microscope for multiple line gratings on a MoSi photomask that have linewidths of nominally 66 nm to 72 nm with a 2 nm increment. Methodology, details for experiments, and sensitivity measurement results are presented with optimal illumination configurations for improving sensitivity.

2. METHODOLOGY FOR DIMENSIONAL METROLOGY

Conventional imaging microscopy has a relatively wide field of view for imaging the targets, though the imaging resolution is limited due to the diffraction limit. Scatterometry is widely used to measure the sub-wavelength dimensions of nanoscale features using scattered intensity distributions containing dimensional information. Using a variety of incidence angles and wavelengths, measured intensities are fit to models generated based on electromagnetic simulation to determine geometrical parameters [10]. Scatterfield imaging microscopy can combine the angular illumination capability of the scatterometry technique and the imaging capability of the conventional imaging microscopy into one platform as shown in Fig. 1. This combination allows manipulation of the illumination angles and shapes that can help more information from nanoscale features through capturing images and potentially varying the focus. By using this method, the three-dimensional scattered fields at the sample are tailored to yield scattered far field images with high sensitivity for improved measurements.

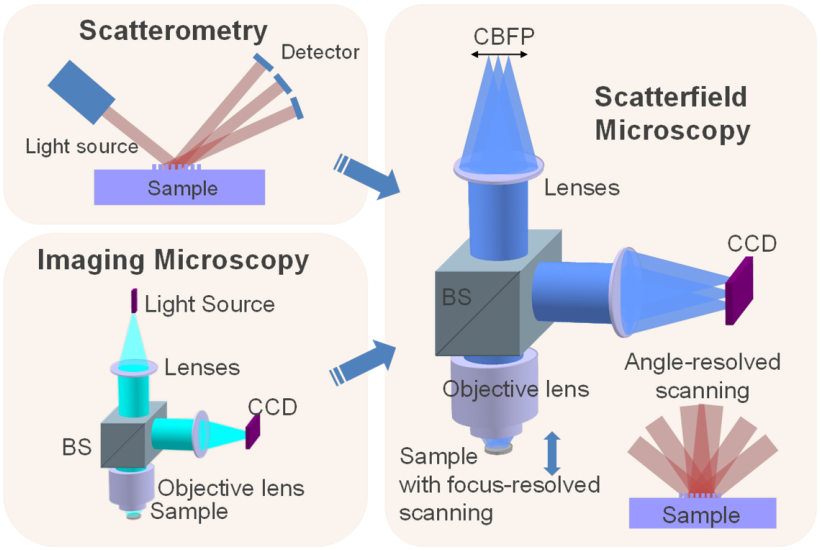

Fig. 1. Schematic of angle-resolved scatterfield imaging microscopy with focus variation.

Tailoring the fields scattered from the sample in scatterfield imaging microscopy is performed by controlling the illumination shape at a conjugate plane of the back focal plane (CBFP) of the objective lens according to the Köhler illumination principle. Fig. 2 shows a schematic of illumination engineering for scatterfield imaging that can be performed at the CBFP. Assuming that the optical system has a Köhler configuration for illumination, a diverging beam from a position at the CBFP illuminates the sample plane as a collimated beam at a corresponding angle. Based on this relationship between the lateral position and the illumination angle, the illumination beam shape can be manipulated by placing apertures designed for specific angles of incidence or by scanning a finite aperture.

This capability has been applied recently to the characterization of tool functions for quantitative nanoscale feature measurement based on parametric modelling analysis. Tool functions for characterizing the illumination and collection path deviations and errors are obtained as intensity functions of illumination angle by scanning a finite aperture at the CBFP [11]. These tool functions are ultimately used to adjust simulated scattered fields for improved fitting to obtain nanoscale feature parameters such as linewidth, height, or sidewall angle based on the captured far field scattered images at the image plane. Using a visible light scatterfield imaging microscope (λ= 450 nm), NIST researchers performed model-based CD measurements for finite grating structures of sub-20 nm silicon-on-silicon lines utilizing a Fourier normalization method which utilizes these tool functions [8]. Scattered field images captured at the image plane were compared against simulation data that were normalized by the instrument characterization and parametric fitting with

sub-nanometer uncertainties. Observing the profiles of these nanoscale features, a small illumination numerical aperture leads to a high ringing at the edges of a relatively large target (100-line grating) and an interference between fields scattered by both edges of a small targets (30-line finite grating). These edge effects may make the scatterfield imaging measurements sensitive to linewidth variations. A low partial coherence factor (0.13/0.95) imposed on the illumination of the optical system triggered these edge effects and could be related to the sensitivity of the parametric measurements using the scatterfield imaging microscopy technique, thus this work investigates the interplay among the edge effects, dimensional sensitivity, and partial coherence in a scatterfield imaging system.

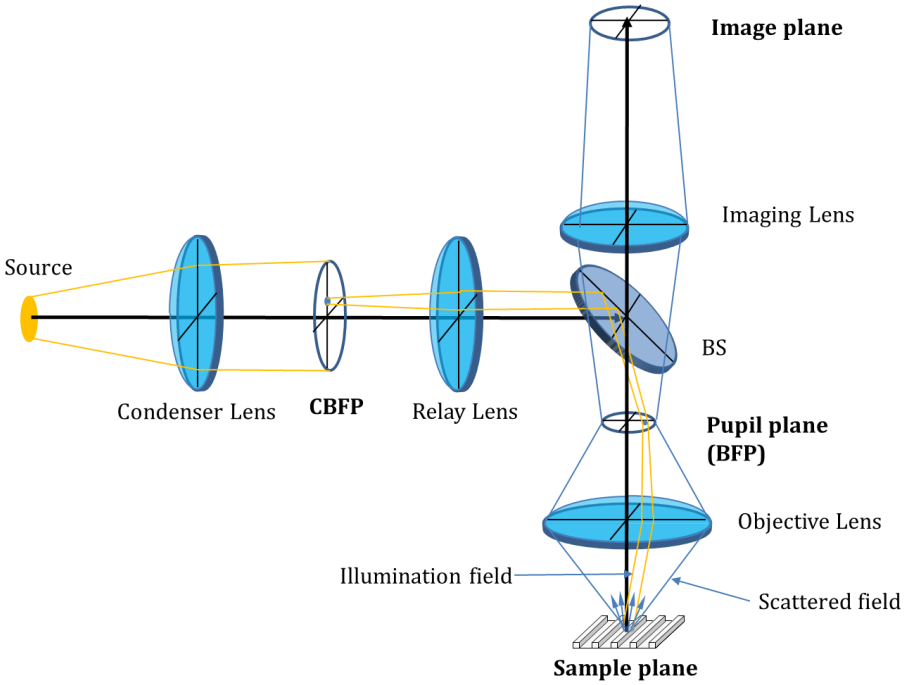

Fig. 2. Illumination engineering schematic for scatterfield imaging using CBFP.

The partial coherence factor $\sigma = NA_{ill} / NA_{col}$, as a metric signifying illumination partial coherence degree in the optical imaging system, is long-established to be important for improving image quality in imaging microscopy system and in lithography exposure process [12-16]. Fig. 3 (a) shows variations in the intensity profiles at a step edge as a function of partial coherence factor [17]. A lower partial coherence factor signifies higher partial coherence generating more ringing effects at the edge. If the edge of a nanoscale grating is considered, the intensity profiles as a function of the partial coherence factor will consist of overshoot at the edge and flat intensity variations at the grating area, as shown in Fig. 3(b). This phenomenon may allow the estimation of measurement sensitivity for the gratings with various linewidths and partial coherence of the imaging system.

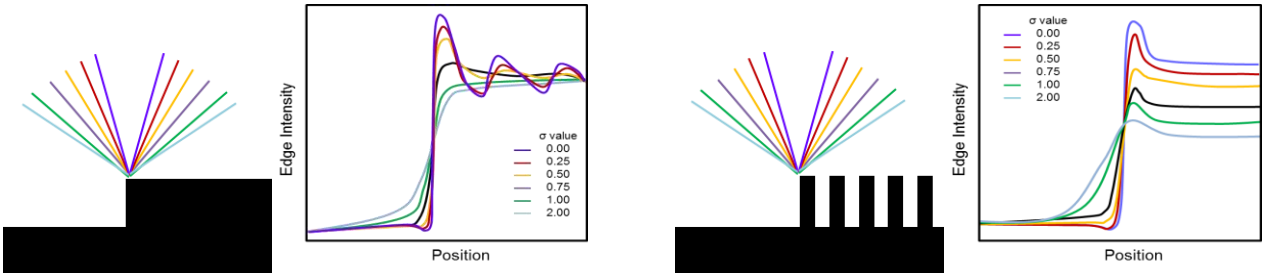

(a) At a step edge

(b) At the edge of multiple lines

Fig. 3. Schematic of hypothetical scattered intensity profiles at the edge for two types of steps.

In this work, measurement of the line and space structure is improved by imaging of the edge area, including both the grating and the substrate. Scatterfield imaging microscopy has an advantage that the imaging area has a relatively large

field of view, which can cover the substrate and grating areas simultaneously as shown in Fig. 4. These capabilities for positioning and spatial selectivity within an image both are useful for measuring the relative signal intensity variations from different linewidth gratings. The normalized signal intensity of the grating area is obtained as the ratio of intensities scattered from the grating and reflected from the substrate. By comparing these relative intensities for various grating linewidths using the substrate as a reference, measurement sensitivity analysis can be performed without modeling. The scattered intensity from the grating varies with the grating's geometric parameters such as linewidth and pitch, with dominant 0-th order scattering away from the edge and a continuum of scattered orders from the grating area. These variations can be used to estimate the sensitivity as a function of partial coherence.

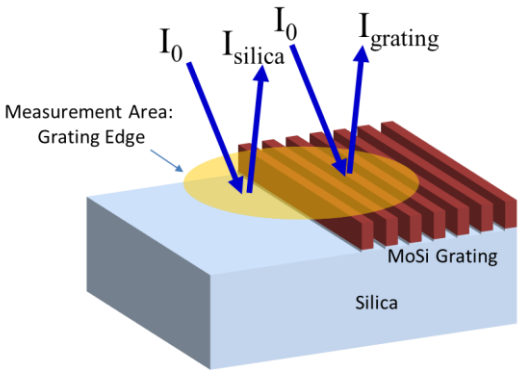

$$I_{norm} = \frac{I_{grating}}{I_{silica}}$$

$$I_{silica} = r_{silica} I_0$$

Fig. 4. Edge imaging method for differentiating scattered intensities from grating area.

3. EXPERIMENTATION

The NIST 193 nm scatterfield imaging microscope system uses an ArF excimer laser as a source, which is the actinic source used for the deep ultraviolet (DUV) immersion lithography exposure process. The microscope adopts a catadioptric objective lens that has an NA of 0.13-0.74, which has a central reflection mirror that blocks light within a numerical aperture of 0.13. The instrument is designed to have a relatively large telecentric CBFP of a diameter of 11.6 mm for enhancing the controlling of the illumination shape as shown in Fig. 5 (a). Various apertures for illumination engineering are placed at the CBFP.

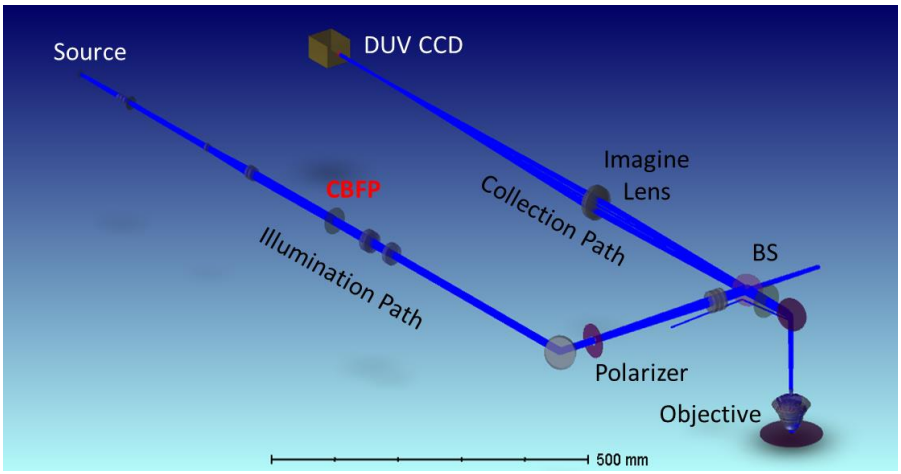

(a) Optics designed

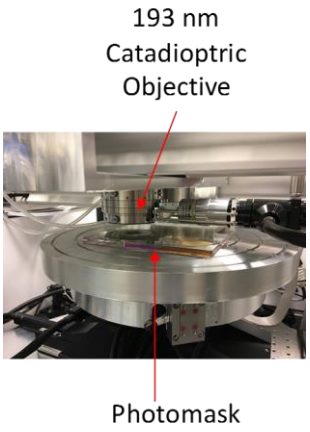

(b) Photomask on the stage

Fig. 5. The NIST 193 nm scatterfield imaging microscope platform.

To engineer the illumination in terms of partial coherence using this DUV scatterfield imaging microscope, three kinds of illuminations are created by three basic aperture shapes: horizontally rectangular, vertically rectangular, and circular apertures, as shown in Fig. 6. Partial coherence can be altered by varying the size of these apertures. For horizontally rectangular apertures, the y-direction illumination angle is both narrow and constant, while the x-direction angle is

varied by changing the length D_x. For vertically rectangular apertures, the y-direction angle covers the full NA, but the x-direction angle is varied by changing the length D_x. For circular apertures, all radial angles are varied with aperture diameter D_x. These aperture size variations are designed to effectively test the interactions of the shaped illumination beams with the grating line for both directions.

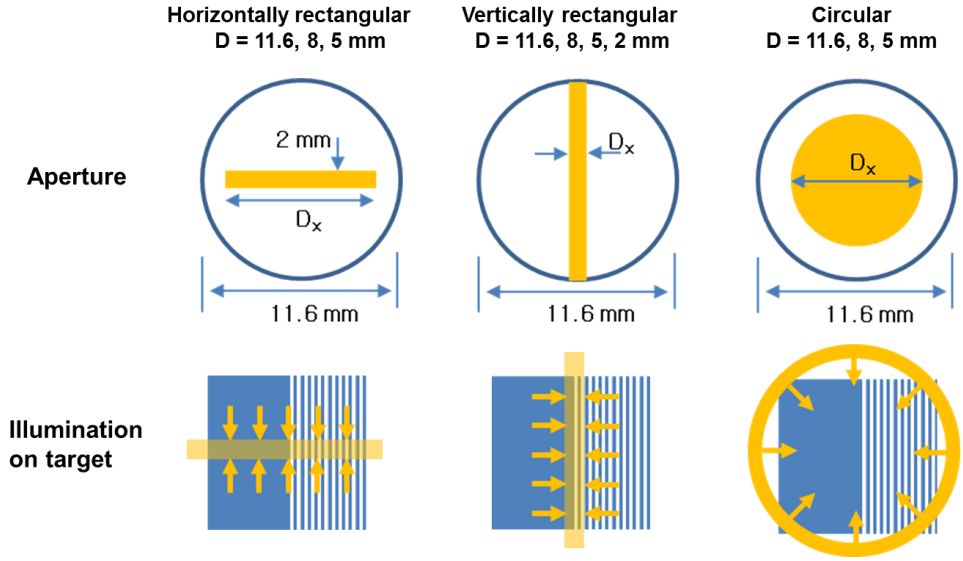

Fig. 6. Apertures for engineering the illumination by varying the partial coherence.

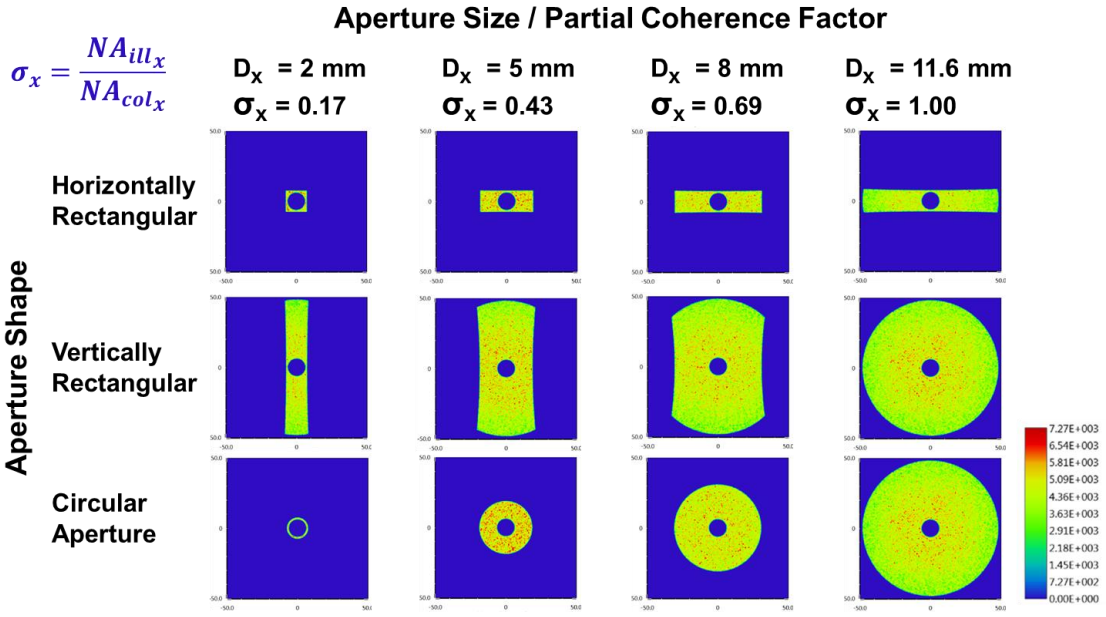

Fig. 7. Simulated angular illumination with respect to the partial coherence factors σ_x.

Using these apertures, angular illumination conditions have been simulated with the optics designed as shown in Fig. 7. The picture array shows the angular illumination shapes at the sample plane in the angle domain as a function of the partial coherence factor for values between 0.17 and 1.0. The partial coherence factor σ_x is varied from 0.17 to 1. The central obscurations are observed due to the central mirror reflection inside of the catadioptric objective lens. The illuminations at a partial coherence factor of 0.17 for the horizontally rectangular and circular apertures yield very small

amounts of energy for illumination, which leads to low signal to noise ratios on the scattered intensity profiles, and therefore, are excluded from the experiments.

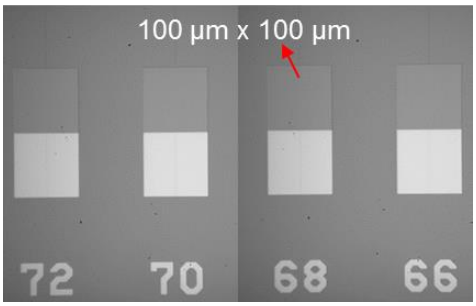

(a) Wide-view optical microscope images

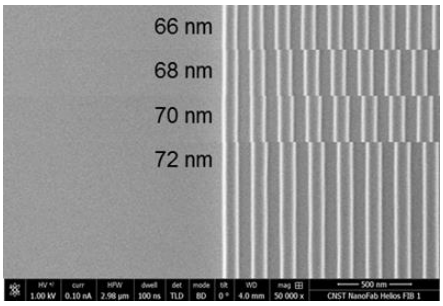

(b) Focused Ion Beam images

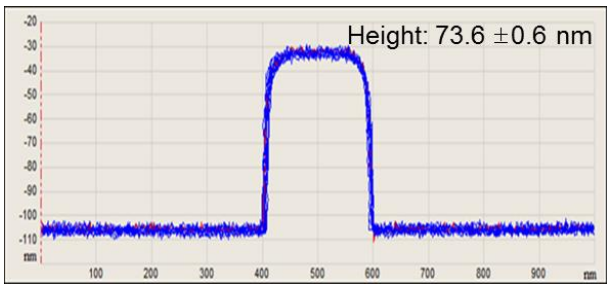

(c) AFM profile of a line extension

Nominal linewidth (nm)	Measured linewidth (nm)	Standard deviation (nm)
66	63.49	1.17
68	65.59	1.17
70	67.96	1.17
72	69.89	1.17

(d) Linewidth values measured with AFM

Fig. 8. Target images captured by various metrology tools.

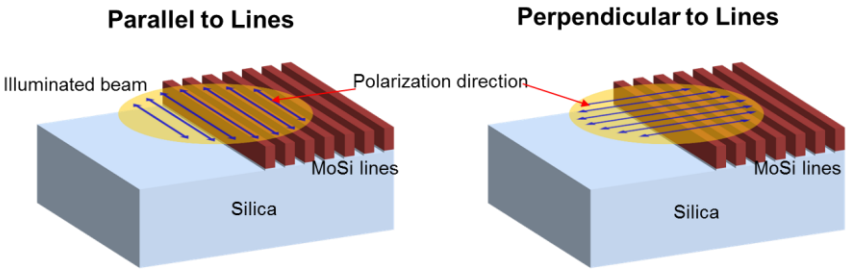

(a) Polarization parallel to lines

(b) Polarization perpendicular to lines

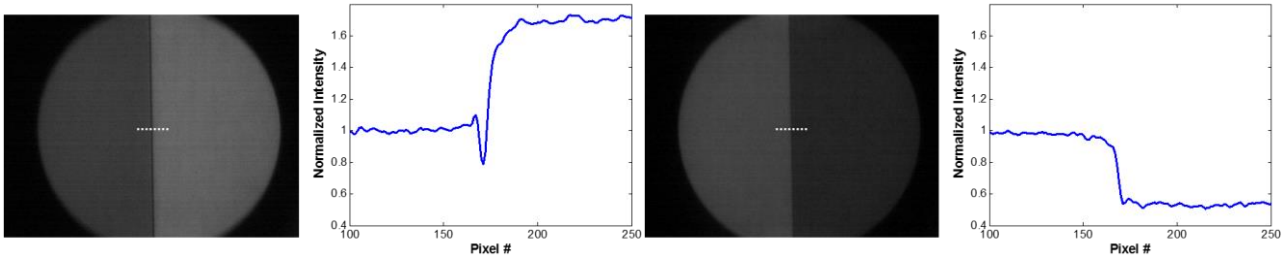

(c) Reflected intensity for parallel polarization

(d) Reflected intensity for perpendicular polarization

Fig. 9. Dependence of edge intensity profiles on illumination polarization.

Sensitivity measurements have been performed for MoSi line gratings on a silica substrate with designed linewidths of 66 nm to 72 nm with 2 nm variation and a 1:1 line/space ratio. Such photomask targets are widely used for lithographic imaging with the phase shift mask technique [18,19]. Fig. 8 shows images taken with a visible-light microscope with a

wide field of view, a focused ion beam (FIB) microscope, and an atomic force microscope (AFM) as reference measurements. The line grating area is 100 μm x 100 μm and each grating has line extension at the center to allow linewidth measurement using AFM as shown in Fig. 8 (a). Gradual variations for each linewidth are shown as an overlapped figure in Fig. 8 (b). The line heights are measured at 73.6 ± 0.6 nm with varied actual linewidths between 63.5 and 69.9 nm as shown in Fig. 8 (c) and (d).

Because the scattered light from gratings is sensitive to the polarization of the incident beam, edge profiles have been measured using two illumination polarizations. Fig. 9 shows the scattered intensity profiles at the edge area for the two orthogonally polarized illumination beams. The reflected intensities between the substrate (left) and the grating (right) change with respect to polarization direction: the intensity at the substrate is lower than at the grating for parallel polarization, while the intensity at the substrate is higher than at the grating for perpendicular polarization, as shown in Fig. 9 (c) and (d). The intensity changes over the silica area are due to the different reflectivity distribution for incident beam angle with different polarizations, which can be calculated from the Fresnel equation. But the grating area intensity changes are due to the scattering interactions among the lines and with the silica substrate.

4. RESULTS AND DISCUSSION

To better measure intensity differentiations among sets of line gratings, intensity profiles were collected for both focused and defocused positions by moving the sample along the z axis as shown in Fig. 10. Each column shows a set of different focus intensity profiles of the 4 different gratings shown in the FIB images inset, varying the target z-position over a range of 2 μm with 1 μm steps and varying the partial coherence factor from 0.17 to 1. A set of 4 intensity distributions for 4 gratings are used to calculate the sensitivity at a specific focus and partial coherence. Edge signal shapes follow trends that are typical of partial coherence variation at a step edge, following the trends shown in Fig. 3 (b). It is observed that the stronger signal intensity variations among the gratings occur at the edges with increased overshoot effects as the partial coherence factor decreases, which signifies increasing partial coherence. Also, the normalized intensity difference between the substrate and the grating areas become larger as the partial coherence increases.

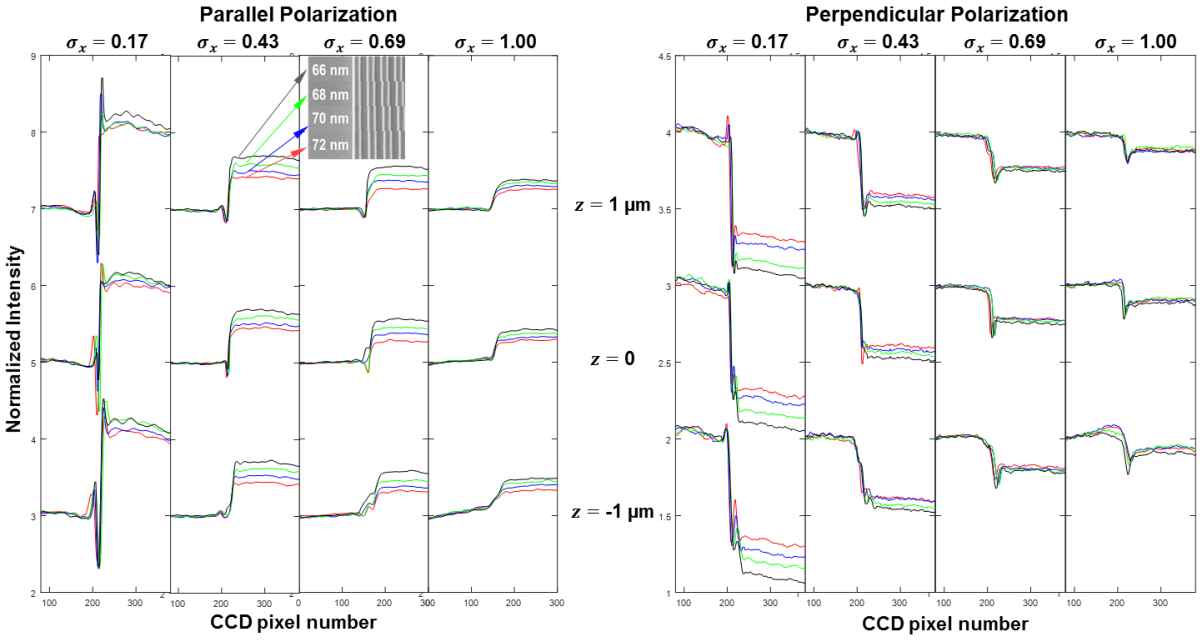

Fig. 10. Edge intensity signals along the grating linewidth and pitch variations in z position variation.

From these intensity distribution variations, empirical sensitivities are calculated for the different illumination instances as shown in Fig. 7 apart from model-based sensitivity analysis [20]. The sensitivity, μ is defined as ratio between the measurand difference Δl and the signal to noise ratio δs for two targets to be measured [21]. The measurands in this analysis are the linewidth values measured by AFM and the signal to noise ratio values are calculated using the mean

intensity difference $\overline{I_2} - \overline{I_1}$ and the standard deviation averages which are obtained from repeated measurements. Note, the 1:1 correspondence of the line and spaces ties linewidth to pitch.

$$\mu = \frac{\Delta l}{\delta s}, \qquad \text{where } \delta s = \frac{abs(\bar{I}_2 - \bar{I}_1)}{\sqrt{\frac{1}{2}\left(std_{I_2}^2 + std_{I_1}^2\right)}}$$

The grating structures for sensitivity measurements either have varied linewidths with a fixed pitch or varied linewidths with varied pitches. For the former, the intensity signal varies only due to scattered field distributions from line geometries as the angles of diffraction orders are fixed. For the latter, the intensity signal varies as field distributions scattered by both line geometries and varied angle of high order diffraction beam due to pitch. In this sensitivity analysis, we used various grating structures, each with its own linewidth and pitch. While linewidth and line geometry may influence the optical response, the intensity variations in this paper are presumed to be due to the pitch variations. And thus the sensitivity analysis is based on the latter case.

Using this empirical sensitivity concept, the sensitivities as a function of the partial coherence factor are obtained from the variations in the normalized intensity distributions as shown in Fig. 11. The graphs summarize the mean intensity results for all investigated cases of apertures, vertically rectangular, horizontally rectangular, and circular. Each point is mean value for repeated measurements and the error bar for each point is the standard deviation. Separations and standard deviations on each graph lead to the sensitivity variations. The vertical aperture shows higher signal variations that are acceptable. These scattered intensity data from the three aperture shape designs, two polarizations, various partial coherence factors, have been processed to yield sensitivity data for three focus positions: at the substrate and one micrometer above and below the substrate.

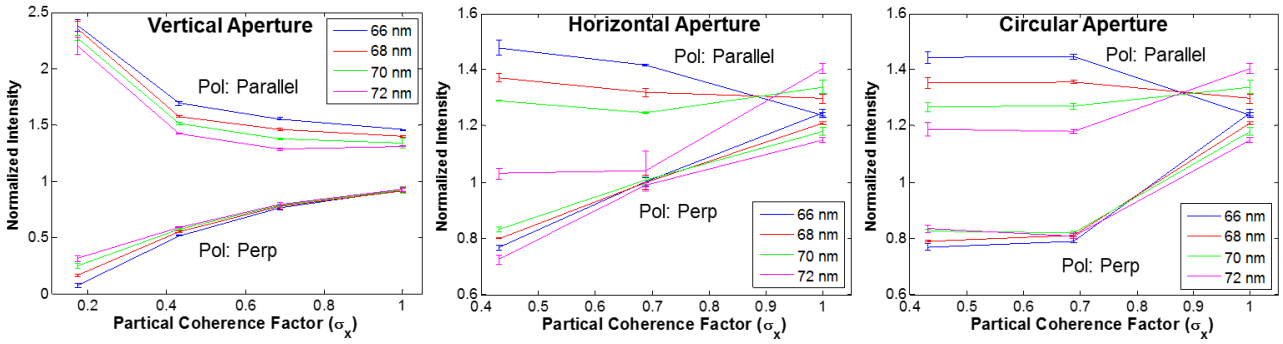

Fig. 11. Normalized scattered intensity signals along the partial coherence factor: each point is mean value for repeated measurements and the error bar for each point is the standard deviation.

Good (< 0.3 nm) Sufficient (0.3 - 0.5 nm)

Sample Position in Z			-1 µm				0 µm				+1 µm			
Partial Coherence Factor (σ_x)			0.17	0.43	0.69	1	0.17	0.43	0.69	1	0.17	0.43	0.69	1
Vertical Aperture	Parallel Pol	Mean	3.055	0.343	0.369	1.222	2.724	0.272	0.249	1.332	2.96	0.441	0.234	1.252
		Std	1.627	0.17	0.189	0.898	2.142	0.087	0.028	1.069	1.662	0.096	0.086	1.254
	Perpendicular Pol	Mean	0.493	0.704	3.935	13.07	0.52	0.494	4.862	13.69	0.372	0.205	3.044	7.514
		Std	0.226	0.386	0.994	10.34	0.197	0.243	4.027	6.056	0.215	0.049	1.137	3.295
Horizontal Aperture	Parallel Pol	Mean		0.543	0.459	1.097		0.283	0.351	0.721		0.391	0.498	0.694
		Std		0.303	0.141	0.626		0.164	0.121	0.353		0.217	0.113	0.404
	Perpendicular Pol	Mean		0.617	16.71	0.77		0.34	9.133	0.669		0.641	6.579	1.17
		Std		0.383	23.63	0.275		0.087	9.108	0.17		0.429	1.671	0.411
Annular Aperture	Parallel Pol	Mean		0.501	0.369	1.097		0.48	0.232	0.721		0.372	0.229	0.694
		Std		0.242	0.192	0.626		0.021	0.036	0.353		0.127	0.092	0.404
	Perpendicular Pol	Mean		1.192	1.459	0.77		1.228	1.23	0.669		1.121	5.593	1.17
		Std		0.618	1.025	0.275		1.138	0.626	0.17		0.221	6.505	0.411

Fig. 12. Sensitivity estimation for partial coherence factor

Fig. 12 shows a metric for determining empirical sensitivity that is applied for each aperture case, polarization, and linewidth. Some of the entries are marked as yellow and green, indicating a sensitivity between 0.3 nm and 0.5 nm and sensitivities less than 0.3 nm, respectively. Agreeing with the graphs in Fig. 11, the illuminations using vertical aperture yield better sensitivities more frequently than the other cases. From these data, in general the optimal illumination conditions for scatterfield imaging measurements consists of a vertical aperture, parallel polarization, and medium partial coherence factor range of about $\sigma = 0.4 \sim 0.7$. Note, the best observed sensitivity, however, is found at 1 micrometer above the substrate using perpendicular polarization.

5. CONCLUSIONS

We investigated empirical sensitivity for a set of MoSi photomask targets with respect to partial coherence using DUV scatterfield imaging microscopy at a wavelength of 193 nm, concluding that partial coherence impacts dimensional measurement sensitivity for scatterfield metrology. The higher partial coherence results in stronger signal intensities at the grating area and improved sensitivities for these targets could be found by tailoring the partial coherence. In this experiment, the optimal illumination condition consists of a vertical rectangle with polarization parallel to the grating lines and a partial coherence factor range between 0.4 ~ 0.7. Optimized measurement sensitivity for scatterfield imaging microscopy is less than 0.3 nm with uncertainties of 0.1 nm or better. Additional target designs should be investigated, analyzing linewidth sensitivity with respect to partial coherence using targets with fixed pitch and varying linewidths. Based on this empirical sensitivity study, it is projected that the DUV scatterfield imaging microscopy technique is feasible to measure nanoscale critical dimensions with sub-nanometer sensitivity, required for advanced CD measurements based on electromagnetic parametric model.

REFERENCES

[1] J. M. Shalf and R. Leland, "Computing beyond Moore's Law," Computer **48**(12), 14-23 (2015).

[2] M. Asano, R. Yoshikawa, T. Hirano, H. Abe, K. Matsuki, H. Tsuda, M. Komori, T. Ojima, H. Yonemitsu, A. Kawamoto, "Metrology and inspection required for next generation lithography," Jpn. J. Appl. Phys. **56**, 06GA01 (2017).

[3] L. Sun, T. Kohyama, K. Takeda, H. Nozawa, Y. Asakawa, T. Kagalwala, G. Lobb, F. Mont, X. Dai, S. Pal, W. Wang, J. Kye, F. Goodwin, "High throughput and dense sampling metrology for process control," Proc. SPIE **10145**, 101452D (2017).

[4] R. M. Silver, T. Germer, R. Attota, B. M. Barnes, B. Bunday, J. Allgair, E. Marx, J. Jun, "Fundamental limits of optical critical dimension metrology: a simulation study," Proc. SPIE **6518**, 65180U (2007).

[5] R. M. Silver, B. M. Barnes, R. Attota, J. S. Jun, M. T. Stocker, E. Mark, H. J. Patrick, "Extending the limits of image-based optical metrology," Appl. Opt. **46**, 4248-4257 (2007).

[6] B. M. Barnes, R. Attota, R. Quintanilha, M. Y. Sohn, R. M. Silver, "Characterizing a scatterfield optical platform for semiconductor metrology," Meas. Sci. Technol. **22**, 024003 (2010).

[7] B. M. Barnes, R. Quintanilha, M. Y. Sohn, H. Zhou, R. M. Silver, "Optical illumination optimization for patterned defect inspection," Proc. SPIE **7971**, 79710D-1 (2011).

[8] J. Qin, R. M. Silver, B. M. Barnes, H. Zhou, R. Dixson, M-A. Henn, "Deep subwavelength nanometric image reconstruction using Fourier domain optical normalization," Light-Sci. Appl. **5**, e16038 (2016).

[9] H. H. Hopkins, "On the diffraction theory of optical images," Proc. Royal Soc. London Series A, **217**(1130) 408-432 (1953).

[10] C. J. Raymond, *et. al.*, "Multiparameter grating metrology using optical scatterometry," J. Vac. Sci. Technol. B **15**, 361 (1997).

[11] J. Qin, R. M. Silver, B. M. Barnes, H. Zhou, F. Goasmat, "Fourier domain optical tool normalization for quantitative parametric image reconstruction," Appl. Opt. **52**(26) 6512-6522 (2013).

[12] E. C. Kintner and R. M. Sillitto, "Edge-ringing in partially coherent imaging," Opt. Acta **24**(5), 591-605 (1977).

[13] M. Singh, H. Lajunen, J. Tervo, J. Turunen, "Imaging with partially coherent light: elementary-field approach," Opt. Express **23**(22), 244084 (2015).

[14] B. Smith, "The saga of sigma: Influences of illumination throughout optical generations," Proc. SPIE **9052**, 905204 (2008).

[15] X. Ma and G. Arce, "Binary mask optimization for inverse lithography with partially coherent illumination," J. Opt. Soc. Am. A **25**, 2960 – 2970 (2008).
[16] P. Naulleau, *et. al.*, "Sub-70 nm extreme ultraviolet lithography at the advanced light source static microfield exposure station using the engineering test stand set-2 optic," J. Vac. Sci. Technol. B **20**(6), 2829 – 2833 (2002).
[17] S. M. Shakeri, L. J. Vliet, S. Stallinga, "Impact of partial coherence on the apparent optical transfer function derived from the response to amplitude edges," Appl. Opt. **56**(12), 3518 (2017).
[18] W. Ahn, et. al., "Development of high-transmittance phase-shifting mask for ArF immersion lithography," Proc. SPIE **9658**, 965808 (2015).
[19] S. Zhang, et. al., "Performance comparison between attenuated PSM and Opaque MoSi on Glass (OMOG) mask in sub-32nm Litho Process," ECS Trans. **44**(1), 249-256 (2012).
[20] P. Vagos, J. Hu, Z. Liu, S. Rabello, "Uncertainty and sensitivity analysis and its applications in OCD measurements," Proc. SPIE **7272**, 72721N (2009).
[21] M. Stocker, B. M. Barnes, M. Sohn, E. Stanfield, R. M. Silver, "Development of large aperture projection scatterometry for catalyst loading evaluation in proton exchange membrane fuel cells," J. Power Sources **364**, 130-137 (2017).